An Efficient Method to Determine Green's Functions of a Two-Dimensional Photonic Crystal Excited by a Line Source—The Phased-Array Method

Christophe Caloz, Anja K. Skrivervik, and Fred E. Gardiol, *Life Fellow, IEEE*

***Abstract*—A novel and efficient method to determine Green's functions in photonic crystals (PCs), i.e., the phased-array method (PAM), is presented. The PAM is a combination of the plane-wave method and the array-scanning method, which is both more flexible and computionally faster than the eigenmodes expansion method. A complete derivation of the electric- and magnetic-field Green's functions associated, respectively, with an infinite electric and magnetic current line exciting a two-dimensional PC is given. Although the developments are presented only for a line source, the PAM can be extended to a dipole source. Thus, the PAM represents a promising method for the analysis of printed-circuit elements or antennas on PC materials. Numerical results for the Green's functions are shown for different positions of the source and a discussion about radiation patterns, asymptotic behaviors, and convergence characteristics is proposed.**

***Index Terms*—Array scanning method, Green's functions, phased-array method, photonic bandgaps, photonic crystals, plane-wave method.**

I. Introduction

OVER THE last decade, photonic crystals (PCs), artificial periodic structures made of dielectric or metallic materials, have drawn significant attention because of their ability to exhibit photonic bandgaps (PBGs), i.e., frequency bands in which no electromagnetic energy can propagate [1]–[5]. The advances in material processing technology and the scalability of PCs to a wide range of frequencies have lead to a vast number of promising applications, not only in the optical range, where research on PCs started in the early 1990s, but also at the microwave and millimeter-wave frequencies. Among these applications, we can mention high-Q cavities and filters [6], low-loss bent waveguides [7], light-emitting diodes [8], low-threshold lasers [9], high-impedance surfaces [10], and a novel class of microstrip lines, filters, and antennas [11]–[13]. In the future, the utilization of all-dielectric PCs as substrates for microstrip planar antennas will be of particular interest when going up to millimeter frequencies. In this application the PC substrate should filter out the spurious surface waves that would propagate in a homogeneous substrate [14], without introducing prohibitive losses like metallic cavities do and, therefore, increase the gain and reduce the sidelobe level of the overall antenna.

Manuscript received August 4, 1999; revised August 4, 2000.

C. Caloz is with the Electrical Engineering Department, University of California at Los Angeles, Los Angeles, CA 90095 USA.

A. K. Skrivervik and F. E. Gardiol are with the Laboratoire d'Électromagnétisme et d'Acoustique, École Polytechnique Fédérale de Lausanne, Lausanne 1015, Switzerland (e-mail: fred.gardiol@urbanet.ch).

Publisher Item Identifier S 0018-9480(02)04050-4.

New wave theories and computational techniques have become necessary to design novel devices and components associated with PCs. The existing analytic and numerical methods, including the plane-wave method (PWM) [15], [16], the finite-difference method, and the finite-element method, are limited either to fully periodic structures or highly localized modes. There is, therefore, a need for computational schemes yielding the field solution of integrated-circuit components interaction with dielectric periodic materials. A very general method, consisting of a vector integral equation in conjunction with an array scanning method (ASM), has been presented in [17] to bridge this gap. In this method, the periodic implants of the PC structure are modeled by equivalent displacement currents, which are determined by a method-of-moments procedure. In the present paper, we propose a different approach, in which the information on periodicity is included directly in the Green's function, i.e., the phased-array method (PAM), which should soon be applicable to microstrip structures.

The PAM is a combination of the PWM and ASM [18], [17]. In contrast to the modal approach of the eigenmodes expansion method (EEM) [19], [20], it directly solves the inhomogeneous dyadic wave equation for the auxiliary problem of a phased array of sources that share the periodicity of the PC. The permittivity is still expanded in a Fourier series as in the EEM, but in the PAM, the expansion over Bloch–Floquet harmonics applies to the periodic Green's functions of the auxiliary problem, and not to the field modes. Once these periodic Green's functions have been determined by solving a matrix system for their coefficients, the actual Green's functions are obtained by the ASM, which transforms the fields due to infinite phased arrays to those due to a single δ source. The PAM is a more efficient and flexible method than the EEM. It is much faster because it involves a more direct computational procedure. Moreover, it does not require the determination of orthonormality and closure relations, which are necessary and sometimes problematic in the EEM. Finally, it works equally well for all field and potential Green's functions, which is not the case for the EEM, where the electric-field Green's functions, for instance, are very cumbersome because they are related to a non-Hermitian operator [19].

In this paper, the PAM is presented in the context of an infinite electric or magnetic current line exciting a two-dimensional (2-D) PC. Two Green's functions, i.e., the electric- and magnetic-field Green's functions associated, respectively, with the infinite electric and magnetic current line, are derived and shown for different positions of the source within the PC. Several features of the Green's functions at in-gap frequencies are pointed out, and the filtering effect of the PBGs is emphasized.

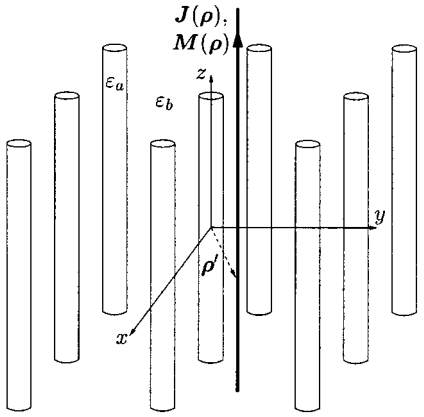

Fig. 1. Infinite electric or magnetic current line ($\boldsymbol{J}(\boldsymbol{\rho})$, $\boldsymbol{M}(\boldsymbol{\rho})$) embedded in a 2-D PC. The line source is located at $\boldsymbol{\rho} = \boldsymbol{\rho}'$.

II. Mathematical Formulation

The structure under consideration is shown in Fig. 1. It consists of an unbounded 2-D PC excited by an infinite current line source, which can be either electric or magnetic. The PAM can be easily applied for any kind of 2-D PC, whatever lattice type (square, hexagonal, rectangular, oblique, honeycomb) and inhomogeneities or "atoms" shapes (circular, square, rectangular, any; compounded) it possesses. For convenience, we will consider a PC constituted of circular atoms of permittivity ε_a embedded in a background medium of permittivity ε_b. The atoms are assumed to be parallel to the z-axis, and the intersections of their axis with the xy-plane form a 2-D-square Bravais lattice [21], as can be seen in Fig. 2. The sites of this lattice are given by the vectors $\boldsymbol{R}_\rho = m\boldsymbol{a}_1 + n\boldsymbol{a}_2$ ($m, n \in \mathbb{Z}$), with the primitive direct vectors $\boldsymbol{a}_1 = a\boldsymbol{e}_x$ and $\boldsymbol{a}_2 = a\boldsymbol{e}_y$, where a represents the lattice constant [see Fig. 2(a)]. The reciprocal lattice vectors then read $\boldsymbol{G}_\rho = h\boldsymbol{b}_1 + k\boldsymbol{b}_2$ ($h, k \in \mathbb{Z}$), with the primitive reciprocal vectors $\boldsymbol{b}_1 = (2\pi/a)\boldsymbol{e}_x$ and $\boldsymbol{b}_2 = (2\pi/a)\boldsymbol{e}_y$ [see Fig. 2(b)], and the Brillouin zone (BZ) is the square surface constituted by the Wigner–Seitz cell of the reciprocal lattice, which is enclosed by the limits $[-\pi/a, \pi/a]$ along both directions x and y [see Fig. 2(c)]. The line is assumed to be parallel to the atoms, and the electric or magnetic currents on this line can be written, respectively, as $\mathbf{J}(\boldsymbol{\rho}) = I\,\delta(\boldsymbol{\rho} - \boldsymbol{\rho}')\boldsymbol{e}_z$ and $\mathbf{M}(\boldsymbol{\rho}) = L\,\delta(\boldsymbol{\rho} - \boldsymbol{\rho}')\boldsymbol{e}_z$, where $\boldsymbol{\rho}'$ represents the position of the line in the transverse xy-plane and I and L denote, respectively, the electric and magnetic current intensity on the line.

It is well known [22], [23] that the modes of an unbounded 2-D PC separate into pure TM (or E-polarized) and TE (or H-polarized) modes, which correspond, respectively, to the (H_x, H_y, E_z) and (E_x, E_y, H_z) nonzero fields components. By reason of symmetry, we can assert that the electric (respectively, magnetic) current line may couple its energy only with TM modes (respectively, TE modes) of the PC, as long as the current along the line is constant. This means that the effective PBGs will be TM PBGs (respectively, a TE PBGs) in the case of the electric (respectively, magnetic) current line, and not necessarily complete TM/TE PBGs. We note that such partial (TM or TE) PBGs are easier to achieve than complete PBGs since the latter ones consist of overlapping of the former ones.

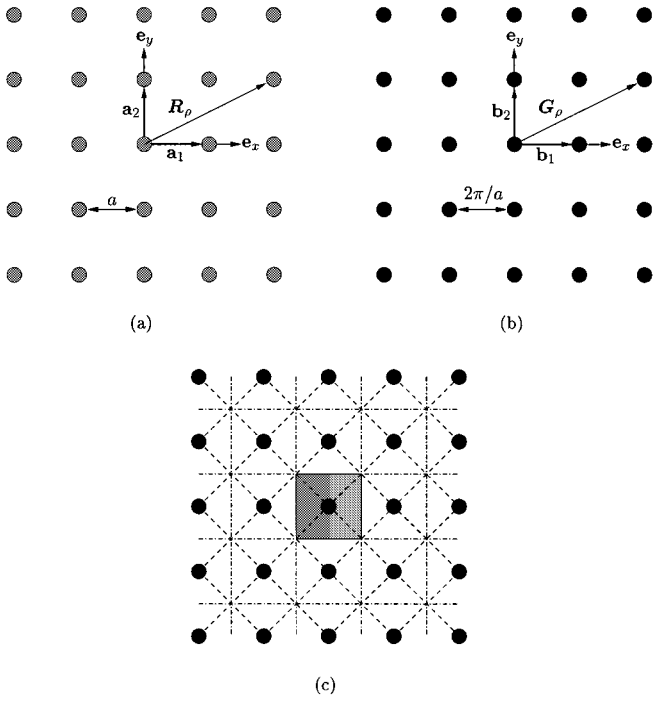

Fig. 2. Square Bravais lattice of lattice constant a. (a) Direct lattice. (b) Reciprocal lattice. (c) Reciprocal lattice and BZ.

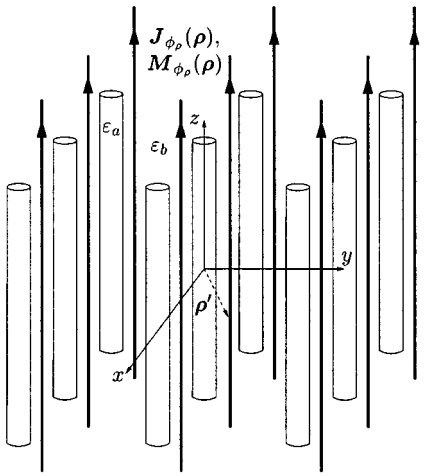

Fig. 3. Phased array of infinite electric or magnetic current lines ($\boldsymbol{J}_{\phi_\rho}(\boldsymbol{\rho})$, $\boldsymbol{M}_{\phi_\rho}(\boldsymbol{\rho})$) embedded in a 2-D PC. Each line source with phasing $e^{j\boldsymbol{k}_\rho \cdot \boldsymbol{R}_\rho}$ is located at $\boldsymbol{\rho} = \boldsymbol{\rho}' + \boldsymbol{R}_\rho$.

Partial PBGs can, therefore, be obtained with lower permittivity contrasts $\Delta\varepsilon$ [$\Delta\varepsilon = \varepsilon_{\max}/\varepsilon_{\min}$, where $\varepsilon_{\max} = \max(\varepsilon_a, \varepsilon_b)$ and $\varepsilon_{\min} = \min(\varepsilon_a, \varepsilon_b)$] and lower filling ratios f_r (ratio of the volume of the atoms over the volume of the complete PC).

The Green's functions for the problem depicted in Fig. 1 cannot be determined in a direct manner because neither aperiodic, nor periodic boundary conditions can be used; the propagation medium being periodic and the source aperiodic. In the context of the PAM, instead of directly solving the problem of the isolated source in the PC, we first consider the geometry shown in Fig. 3, where the PC is excited by an infinite

phased array of current line sources sharing the same periodicity as the PC and possessing progressive phase shifts given by $\phi_{\boldsymbol{\rho}} = \boldsymbol{k}_\rho \cdot \boldsymbol{R}_\rho$, where $\boldsymbol{k}_\rho$ is a phasing vector (see Appendix I). The electric and magnetic lines currents can, therefore, be written as follows:

$$\begin{pmatrix} \boldsymbol{J}_{\phi_\rho}(\boldsymbol{\rho}) \\ \boldsymbol{M}_{\phi_\rho}(\boldsymbol{\rho}) \end{pmatrix} = \begin{pmatrix} J_{\phi_\rho}(\boldsymbol{\rho}) \\ M_{\phi_\rho}(\boldsymbol{\rho}) \end{pmatrix} \boldsymbol{e}_z = \begin{pmatrix} I \\ L \end{pmatrix} \left[\sum_{\boldsymbol{R}_\rho} \delta(\boldsymbol{\rho} - \boldsymbol{\rho}' - \boldsymbol{R}_\rho) e^{j\boldsymbol{k}_\rho \cdot \boldsymbol{R}_\rho} \right] \boldsymbol{e}_z \quad (1)$$

where each line located at $\boldsymbol{\rho} = \boldsymbol{\rho}' + \boldsymbol{R}_\rho$ possesses the phasing $e^{j\boldsymbol{k}_\rho \cdot \boldsymbol{R}_\rho}$.

In this auxiliary phased-array problem, the complete structure is periodic, except for the phasing dependence, which will be used later to return to the original problem. It is, therefore, possible to determine the Green's functions, which will also be periodic, except for the phasing, and which will be referred to by the generic notation $\overline{\overline{G}}_{\rm per}(\boldsymbol{\rho}|\boldsymbol{\rho}'; \boldsymbol{k}_\rho)$.

Once $\overline{\overline{G}}_{\rm per}(\boldsymbol{\rho}|\boldsymbol{\rho}'; \boldsymbol{k}_\rho)$ has been determined, the corresponding Green's function of the original problem $\overline{\overline{G}}(\boldsymbol{\rho}|\boldsymbol{\rho}')$ can be obtained by performing the following integration on the phasing vector $\boldsymbol{k}_\rho$ over the BZ:

$$\overline{\overline{G}}(\boldsymbol{\rho}|\boldsymbol{\rho}') = \frac{1}{S_{BZ}} \int_{BZ} \overline{\overline{G}}_{\rm per}(\boldsymbol{\rho}|\boldsymbol{\rho}'; \boldsymbol{k}_\rho)\, d\boldsymbol{k}_\rho. \quad (2)$$

The integration in (2), which is well known from the phased-array theory [24], [18], represents in effect the superposition of the phased-array solutions corresponding to the phasing $e^{j\boldsymbol{k}_\rho \cdot \boldsymbol{R}_\rho}$. In this mathematical superposition, that is allowed by the physical superposition principle of electromagnetic fields in linear systems, the effects of all the sources are canceled out, except the one of the source possessing a zero phasing, which is to say, the source located at $\boldsymbol{\rho} = \boldsymbol{\rho}'$. It should be noted that this source does not need to belong to the Wigner–Seitz cell of the direct lattice.

Although the PAM is applicable to any field or potential Green's function, we will restrict ourselves in this paper to the Green's function of the electric field $\boldsymbol{E}$ due to an electric source $\boldsymbol{J}$ and to the Green's function of the magnetic field $\boldsymbol{H}$ due to a magnetic source $\boldsymbol{M}$, which we note, respectively, as $\overline{\overline{G}}_{EJ}$ and $\overline{\overline{G}}_{HM}$. It should be noted that these two problems are *not duals* because of the dissymmetry introduced in Maxwell equations by the space-varying permittivity of the PC. Hence, we expect different behaviors for $\overline{\overline{G}}_{EJ}$ and $\overline{\overline{G}}_{HM}$, especially if the PC presents an important permittivity contrast $\Delta\varepsilon$.

The dyadic wave equations relevant to $\overline{\overline{G}}_{EJ_{\rm per}}$ and $\overline{\overline{G}}_{HM_{\rm per}}$ read

$$\nabla \times \nabla \times \overline{\overline{G}}_{EJ_{\rm per}}(\boldsymbol{\rho}|\boldsymbol{\rho}'; \boldsymbol{k}_\rho) - \left(\frac{\omega}{c}\right)^2 \varepsilon_r(\boldsymbol{\rho}) \overline{\overline{G}}_{EJ_{\rm per}}(\boldsymbol{\rho}|\boldsymbol{\rho}'; \boldsymbol{k}_\rho) = -j\omega\mu_0 \overline{\overline{I}} J_{\phi_\rho}(\boldsymbol{\rho})/I \quad (3a)$$

$$\nabla \times \left[\frac{1}{\varepsilon_r(\boldsymbol{\rho})} \nabla \times \overline{\overline{G}}_{HM_{\rm per}}(\boldsymbol{\rho}|\boldsymbol{\rho}'; \boldsymbol{k}_\rho) \right] - \left(\frac{\omega}{c}\right)^2 \overline{\overline{G}}_{HM_{\rm per}}(\boldsymbol{\rho}|\boldsymbol{\rho}'; \boldsymbol{k}_\rho) = -j\omega\varepsilon_0 \overline{\overline{I}} M_{\phi_\rho}(\boldsymbol{\rho})/L \quad (3b)$$

where the expressions of $J_{\phi_\rho}(\boldsymbol{\rho})$ and $M_{\phi_\rho}(\boldsymbol{\rho})$ are given by (1).

Since the dyadic functions $\overline{\overline{G}}_{EJ_{\rm per}}$ and $\overline{\overline{G}}_{HM_{\rm per}}$ are periodic in modulus, they can be expanded over Bloch–Floquet harmonics

$$\begin{pmatrix} \overline{\overline{G}}_{EJ_{\rm per}}(\boldsymbol{\rho}|\boldsymbol{\rho}'; \boldsymbol{k}_\rho) \\ \overline{\overline{G}}_{HM_{\rm per}}(\boldsymbol{\rho}|\boldsymbol{\rho}'; \boldsymbol{k}_\rho) \end{pmatrix} = \boldsymbol{e}_z \sum_{\boldsymbol{G}_\rho} \begin{pmatrix} \tilde{g}_{EJ}(\boldsymbol{\rho}'; \boldsymbol{k}_\rho, \boldsymbol{G}_\rho) \\ \tilde{g}_{HM}(\boldsymbol{\rho}'; \boldsymbol{k}_\rho, \boldsymbol{G}_\rho) \end{pmatrix} e^{j(\boldsymbol{k}_\rho + \boldsymbol{G}_\rho)\cdot(\boldsymbol{\rho} - \boldsymbol{\rho}')} \boldsymbol{e}_z \quad (4)$$

where the $\boldsymbol{G}_\rho$-spectral coefficients $\tilde{g}_{EJ}(\boldsymbol{\rho}'; \boldsymbol{k}_\rho, \boldsymbol{G}_\rho)$ and $\tilde{g}_{HM}(\boldsymbol{\rho}'; \boldsymbol{k}_\rho, \boldsymbol{G}_\rho)$ depend on the position $\boldsymbol{\rho}'$ of the zero-phased source and on the phasing vector $\boldsymbol{k}_\rho$. This Bloch–Floquet spectral expression of the Green's functions is formally analogous to the one presented in [25] for the case of a phased array of dipoles on an *homogeneous* grounded substrate. However, because of the inhomogeneity of the propagation medium, the spectral Green's coefficients will be determined here in a completely different way.

The following amplitude periodicity relations for $\overline{\overline{G}}_{EJ_{\rm per}}$ and $\overline{\overline{G}}_{HM_{\rm per}}$:

$$\begin{pmatrix} \overline{\overline{G}}_{EJ_{\rm per}}(\boldsymbol{\rho}+\boldsymbol{R}_\rho|\boldsymbol{\rho}'; \boldsymbol{k}_\rho) \\ \overline{\overline{G}}_{HM_{\rm per}}(\boldsymbol{\rho}+\boldsymbol{R}_\rho|\boldsymbol{\rho}'; \boldsymbol{k}_\rho) \end{pmatrix} = e^{j\boldsymbol{k}_\rho \cdot \boldsymbol{R}_\rho} \begin{pmatrix} \overline{\overline{G}}_{EJ_{\rm per}}(\boldsymbol{\rho}|\boldsymbol{\rho}'; \boldsymbol{k}_\rho) \\ \overline{\overline{G}}_{HM_{\rm per}}(\boldsymbol{\rho}|\boldsymbol{\rho}'; \boldsymbol{k}_\rho) \end{pmatrix} \quad (5)$$

can be easily verified, taking into account the fact that $e^{j\boldsymbol{G}_\rho \cdot \boldsymbol{R}_\rho} = 1$ by definition [21].

Now that we have found the spectral representations (4) of the Green's functions through the Bloch–Floquet theorem, we still have to determine the corresponding spectral representation of the array currents (1) in order to solve (3). This can be done with the help of the Poisson's sum formula (see Appendix II), which yields

$$\begin{pmatrix} J_{\phi_\rho}(\boldsymbol{\rho}) \\ M_{\phi_\rho}(\boldsymbol{\rho}) \end{pmatrix} = \frac{S_{BZ}}{(2\pi)^2} \begin{pmatrix} I \\ L \end{pmatrix} \left[\sum_{\boldsymbol{G}_\rho} e^{j(\boldsymbol{k}_\rho + \boldsymbol{G}_\rho)\cdot(\boldsymbol{\rho} - \boldsymbol{\rho}')} \right] \quad (6)$$

where S_{BZ} denotes the surface of the BZ.

The last step before passing to the resolution of the wave equations consists in expressing the relative permittivity $\varepsilon_r(\boldsymbol{\rho})$ and the inverse of the relative permittivity $\kappa_r(\boldsymbol{\rho}) = 1/\varepsilon_r(\boldsymbol{\rho})$ functions as Fourier series expansions, which is allowed because these functions are periodic as follows:

$$\begin{pmatrix} \varepsilon_r(\boldsymbol{\rho}) \\ \kappa_r(\boldsymbol{\rho}) \end{pmatrix} = \sum_{\boldsymbol{G}_\rho} \begin{pmatrix} \tilde{\varepsilon}_r(\boldsymbol{G}_\rho) \\ \tilde{\kappa}_r(\boldsymbol{G}_\rho) \end{pmatrix} e^{j\boldsymbol{G}_\rho \cdot \boldsymbol{\rho}} \quad (7)$$

where the terms $\tilde{\varepsilon}_r(\boldsymbol{G}_\rho)$ and $\tilde{\kappa}_r(\boldsymbol{G}_\rho)$ denote, respectively, the Fourier coefficients of $\varepsilon_r(\boldsymbol{\rho})$ and $\kappa_r(\boldsymbol{\rho})$, which are given for circular atoms by

$$\begin{pmatrix}\tilde{\varepsilon}_r(\boldsymbol{G}_\rho)\\ \tilde{\kappa}(\boldsymbol{G}_\rho)\end{pmatrix}=\begin{cases}\begin{pmatrix}\varepsilon_a\\ \dfrac{1}{\varepsilon_a}\end{pmatrix}f_r & \\ \quad+\begin{pmatrix}\varepsilon_b\\ \dfrac{1}{\varepsilon_b}\end{pmatrix}(1-f_r), & \text{if } \boldsymbol{G}_\rho=0\\ \begin{pmatrix}(\varepsilon_a-\varepsilon_b)\\ \left(\dfrac{1}{\varepsilon_a}-\dfrac{1}{\varepsilon_b}\right)\end{pmatrix} & \\ \quad\dfrac{2J_1(G_\rho R_c)}{G_\rho R_c}f_r, & \text{if } \boldsymbol{G}_\rho\neq 0\end{cases} \tag{8}$$

with the filling ratio $f_r=\pi(R_c/a)^2$.

Inserting (4), (6), and (7) into (3) then yields

$$\begin{aligned}&\tilde{\nabla}\times\tilde{\nabla}\times\left[\sum_{\boldsymbol{G}_\rho}\tilde{g}_{EJ}(\boldsymbol{\rho}';\boldsymbol{k}_\rho,\boldsymbol{G}_\rho)e^{j(\boldsymbol{k}_\rho+\boldsymbol{G}_\rho)\cdot(\boldsymbol{\rho}-\boldsymbol{\rho}')}\overline{\overline{I}}_z\right]\\&\quad-\left(\frac{\omega}{c}\right)^2\left(\sum_{\boldsymbol{G}''_\rho}\tilde{\varepsilon}_r\left(\boldsymbol{G}''_\rho\right)e^{j\boldsymbol{G}''_\rho\cdot\boldsymbol{\rho}}\right)\\&\quad\cdot\left[\sum_{\boldsymbol{G}'_\rho}\tilde{g}_{EJ}(\boldsymbol{\rho}';\boldsymbol{k}_\rho,\boldsymbol{G}'_\rho)e^{j(\boldsymbol{k}_\rho+\boldsymbol{G}'_\rho)\cdot(\boldsymbol{\rho}-\boldsymbol{\rho}')}\overline{\overline{I}}_z\right]\\&\quad=-j\frac{\omega\mu_0 S_{BZ}}{(2\pi)^2}\overline{\overline{I}}_z\sum_{\boldsymbol{G}_\rho}e^{j(\boldsymbol{k}_\rho+\boldsymbol{G}_\rho)\cdot(\boldsymbol{\rho}-\boldsymbol{\rho}')}\end{aligned} \tag{9a}$$

$$\begin{aligned}&\nabla\times\left\{\left(\sum_{\boldsymbol{G}''_\rho}\tilde{\kappa}_r\left(\boldsymbol{G}''_\rho\right)e^{j\boldsymbol{G}''_\rho\cdot\boldsymbol{\rho}}\right)\tilde{\nabla}\right.\\&\qquad\left.\times\left[\sum_{\boldsymbol{G}'_\rho}\tilde{g}_{HM}(\boldsymbol{\rho}';\boldsymbol{k}_\rho,\boldsymbol{G}'_\rho)e^{j(\boldsymbol{k}_\rho+\boldsymbol{G}'_\rho)\cdot(\boldsymbol{\rho}-\boldsymbol{\rho}')}\overline{\overline{I}}_z\right]\right\}\\&\quad-\left(\frac{\omega}{c}\right)^2\left[\sum_{\boldsymbol{G}_\rho}\tilde{g}_{HM}(\boldsymbol{\rho}';\boldsymbol{k}_\rho,\boldsymbol{G}_\rho)e^{j(\boldsymbol{k}_\rho+\boldsymbol{G}_\rho)\cdot(\boldsymbol{\rho}-\boldsymbol{\rho}')}\overline{\overline{I}}_z\right]\\&\quad=-j\frac{\omega\varepsilon_0 S_{BZ}}{(2\pi)^2}\overline{\overline{I}}_z\sum_{\boldsymbol{G}_\rho}e^{j(\boldsymbol{k}_\rho+\boldsymbol{G}_\rho)\cdot(\boldsymbol{\rho}-\boldsymbol{\rho}')}\end{aligned} \tag{9b}$$

where $\overline{\overline{I}}_z$ represents the longitudinal projection of the identity dyadic $\overline{\overline{I}}_z=\boldsymbol{e}_z\boldsymbol{e}_z$, and where we have introduced the spectral operator $\tilde{\nabla}\times=j(\boldsymbol{k}_\rho+\boldsymbol{G}_\rho)\times$, which is equivalent to the spatial differential operator $\nabla\times$ as long as it operates only on identical Bloch–Floquet expressions. It should be noted that this is not the case for the first $\nabla\times$ in the second equation because of the interposition of the function $e^{j\boldsymbol{G}''_\rho\cdot\boldsymbol{\rho}}$.

Upon developing the curl terms, substituting $\boldsymbol{G}_\rho=\boldsymbol{G}'_\rho+\boldsymbol{G}''_\rho$, and dividing both sides in (9) by $e^{-j\boldsymbol{G}_\rho\cdot\boldsymbol{\rho}'}$, we obtain

$$\begin{aligned}&\sum_{\boldsymbol{G}_\rho}\left\{(\boldsymbol{k}_\rho+\boldsymbol{G}_\rho)^2\tilde{g}_{EJ}(\boldsymbol{G}_\rho)-\left(\frac{\omega}{c}\right)^2\right.\\&\qquad\left.\cdot\sum_{\boldsymbol{G}'_\rho}\tilde{\varepsilon}_r\left(\boldsymbol{G}_\rho-\boldsymbol{G}'_\rho\right)e^{j(\boldsymbol{G}_\rho-\boldsymbol{G}'_\rho)\cdot\boldsymbol{\rho}'}\tilde{g}_{EJ}(\boldsymbol{G}'_\rho)\right\}\\&\quad\cdot e^{j(\boldsymbol{k}_\rho+\boldsymbol{G}_\rho)\cdot(\boldsymbol{\rho}-\boldsymbol{\rho}')}\\&\quad=-j\frac{\omega\mu_0 S_{BZ}}{(2\pi)^2}\sum_{\boldsymbol{G}_\rho}e^{j(\boldsymbol{k}_\rho+\boldsymbol{G}_\rho)\cdot(\boldsymbol{\rho}-\boldsymbol{\rho}')}\end{aligned} \tag{10a}$$

$$\begin{aligned}&\sum_{\boldsymbol{G}_\rho}\left\{\sum_{\boldsymbol{G}'_\rho}\tilde{\kappa}_r\left(\boldsymbol{G}_\rho-\boldsymbol{G}'_\rho\right)e^{j(\boldsymbol{G}_\rho-\boldsymbol{G}'_\rho)\cdot\boldsymbol{\rho}'}\left(\boldsymbol{k}_\rho+\boldsymbol{G}_\rho\right)\right.\\&\qquad\left.\cdot\left(\boldsymbol{k}_\rho+\boldsymbol{G}'_\rho\right)\tilde{g}_{HM}\left(\boldsymbol{G}'_\rho\right)-\left(\frac{\omega}{c}\right)^2\tilde{g}_{HM}(\boldsymbol{G}_\rho)\right\}\\&\quad\cdot e^{j(\boldsymbol{k}_\rho+\boldsymbol{G}_\rho)\cdot(\boldsymbol{\rho}-\boldsymbol{\rho}')}\\&\quad=-j\frac{\omega\varepsilon_0 S_{BZ}}{(2\pi)^2}\sum_{\boldsymbol{G}_\rho}e^{j(\boldsymbol{k}_\rho+\boldsymbol{G}_\rho)\cdot(\boldsymbol{\rho}-\boldsymbol{\rho}')}\end{aligned} \tag{10b}$$

where the $(\boldsymbol{\rho}';\boldsymbol{k}_\rho)$ dependence of the spectral coefficients has been dropped for simplicity.

By identification we can leave out the summations $\sum_{\boldsymbol{G}_\rho}$ and the exponentials $e^{j(\boldsymbol{k}_\rho+\boldsymbol{G}_\rho)\cdot(\boldsymbol{\rho}-\boldsymbol{\rho}')}$ in both equations. This can be rigorously justified by multiplying both sides of the equations by $e^{-j\boldsymbol{G}''_\rho\cdot\boldsymbol{\rho}}$, integrating over $\boldsymbol{\rho}$, and using the orthonormality property of the complex exponential. Equation (10) then yield the following matrix systems:

$$\begin{aligned}&(\boldsymbol{k}_\rho+\boldsymbol{G}_\rho)^2\tilde{g}_{EJ}(\boldsymbol{G}_\rho)\\&\quad-\left(\frac{\omega}{c}\right)^2\sum_{\boldsymbol{G}'_\rho}\tilde{\varepsilon}_r\left(\boldsymbol{G}_\rho-\boldsymbol{G}'_\rho\right)e^{j(\boldsymbol{G}_\rho-\boldsymbol{G}'_\rho)\cdot\boldsymbol{\rho}'}\tilde{g}_{EJ}\left(\boldsymbol{G}'_\rho\right)\\&\quad=-j\frac{\omega\mu_0 S_{BZ}}{(2\pi)^2}\end{aligned} \tag{11a}$$

$$\begin{aligned}&\sum_{\boldsymbol{G}'_\rho}\tilde{\kappa}_r\left(\boldsymbol{G}_\rho-\boldsymbol{G}'_\rho\right)e^{j(\boldsymbol{G}_\rho-\boldsymbol{G}'_\rho)\cdot\boldsymbol{\rho}'}\left(\boldsymbol{k}_\rho+\boldsymbol{G}_\rho\right)\\&\qquad\cdot\left(\boldsymbol{k}_\rho+\boldsymbol{G}'_\rho\right)\tilde{g}_{HM}\left(\boldsymbol{G}'_\rho\right)-\left(\frac{\omega}{c}\right)^2\tilde{g}_{HM}(\boldsymbol{G}_\rho)\\&\quad=-j\frac{\omega\varepsilon_0 S_{BZ}}{(2\pi)^2}.\end{aligned} \tag{11b}$$

Once these systems have been solved for a given set $(\boldsymbol{\rho}';\boldsymbol{k}_\rho)$, i.e., once the coefficients $\tilde{g}_{EJ}(\boldsymbol{\rho}';\boldsymbol{k}_\rho,\boldsymbol{G}_\rho)$ and $\tilde{g}_{HM}(\boldsymbol{\rho}';\boldsymbol{k}_\rho,\boldsymbol{G}_\rho)$ have been determined, the periodic Green's functions (4) of the auxiliary problem shown in Fig. 3 are fully

determined, and the Green's functions of the original problem shown in Fig. 1 are obtained with the relation (2)

$$\begin{pmatrix} \overline{\overline{G}}_{EJ}(\boldsymbol{\rho}|\boldsymbol{\rho}') \\ \overline{\overline{G}}_{HM}(\boldsymbol{\rho}|\boldsymbol{\rho}') \end{pmatrix} = \frac{1}{S_{BZ}} \int_{BZ} \left\{ \sum_{\boldsymbol{G}_\rho} \begin{pmatrix} \tilde{g}_{EJ}(\boldsymbol{\rho}';\boldsymbol{k}_\rho,\boldsymbol{G}_\rho) \\ \tilde{g}_{HM}(\boldsymbol{\rho}';\boldsymbol{k}_\rho,\boldsymbol{G}_\rho) \end{pmatrix} \cdot e^{j(\boldsymbol{k}_\rho+\boldsymbol{G}_\rho)\cdot(\boldsymbol{\rho}-\boldsymbol{\rho}')} \overline{\overline{I}}_z \right\} d\boldsymbol{k}_\rho. \tag{12}$$

It is worth emphasizing the generality and flexibility of the PAM. Changing the lattice type necessitates only changing the set of reciprocal lattice vectors $\boldsymbol{G}_\rho$ appearing in the matrix systems (11) and modifying the BZ on which the integral (12) is performed. For example, if we pass to a hexagonal lattice, we just have to change $\boldsymbol{G}_\rho$ to $\boldsymbol{G}_\rho = (2\pi/a)\ [h(\sqrt{3}\mathbf{e}_x + \mathbf{e}_y)/2 + k(\sqrt{3}\mathbf{e}_x - \mathbf{e}_y)/2]$, the filling ratio to $f_r = (2\pi/\sqrt{3})(R_c/a)^2$, and the BZ to the new corresponding hexagonal surface [22]. Changing the atoms shapes requires only the modification of the Fourier coefficients of $\tilde{\varepsilon}_r(\boldsymbol{G}_\rho)$ and $\tilde{\kappa}(\mathbf{G}_\rho)$, which can possess an analytical form like in (8) and for rectangular atoms [26], or a numerical form for more complex shapes.

III. Numerical Results and Discussion

As outlined in the previous section, the effective PBGs associated with an electric current line and, therefore, with G_{EJ} (respectively, with a magnetic current line and, therefore, with $\overline{\overline{G}}_{HM}$) are TM PBGs (respectively, TE PBGs). Since in the case of a square lattice, TM PBGs (respectively, TE PBGs) are favored in PCs constituted of isolated high-ε spots surrounded by a low-ε medium (respectively, of high-ε connected veins surrounding low-ε spots [22]), we consider a PC made of dielectric rods in air for G_{EJ} and a PC made of air holes in a dielectric medium for G_{HM}. The photonic band structures (or dispersion relations) for these two PCs, computed with the PWM, are shown in Fig. 4, where we have defined the normalized frequency $\omega_{\text{norm}} = \omega a/2\pi c = a/\lambda$. In the range of frequencies shown, the lattice of rods exhibits four TM PBGs, extending in the frequency ranges $\omega_{\text{norm}} = [0.22, 0.27], [0.38, 0.46], [0.58, 0.65]$ and $[0.77, 0.80]$, and the lattice of holes exhibits two TE PBGs, extending in the frequency ranges $\omega_{\text{norm}} = [0.30, 0.33]$ and $[0.40, 0.47]$.

The integration in (2) was performed with a standard Gauss–Legendre integration procedure in which convergence has been insured with $N_k = 8$ spectral points in the BZ along both directions k_x and k_y. When not otherwise stated in the figures, the number of plane waves in the expansions (4), (6), and (7), which is also the size of the matrix systems (11), and which we call N_G, was set to 300 for each value of $\boldsymbol{k}_\rho$.

The Green's functions G_{EJ} for $\omega_{\text{norm}} = 0.42$ [$\in$ second TM PBG of Fig. 4(a)] (respectively, G_{HM} for $\omega_{\text{norm}} = 0.45$) [$\in$ second TE PBG of Fig. 4(b)] for the source positions $\boldsymbol{\rho}'/a = (0.0, 0.0)$, $\boldsymbol{\rho}'/a = (0.5, 0.5)$, and $\boldsymbol{\rho}'/a = (0.2, 0.3)$ are shown in Figs. 5–7 (respectively, in Figs. 8–10). Comparing the computed Green's function G_{HM} with the results obtained in [20]

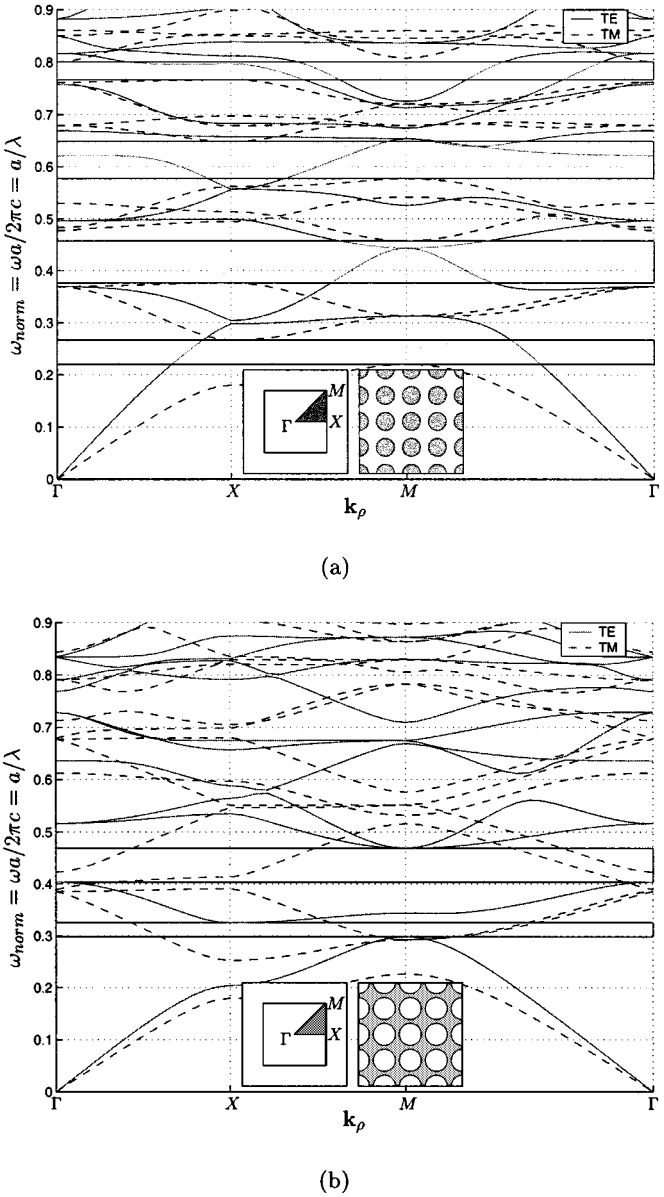

Fig. 4. Photonic band structures of two different square-lattice 2-D PC constituted of HiK-12 ($\varepsilon_r = 12$) and air. The left-hand-side insets show the BZ, with the irreductible zone shaded. The right —hand-side insets represent a scaled cross-sectional view of the dielectric function $\varepsilon_r(\boldsymbol{\rho})$. (a) Lattice of cylindrical rods of radius $R_c = 0.35a$ ($\varepsilon_a = 12, \varepsilon_b = 1$). The shaded bands show the TM PBGs, representing effective PBGs for G_{EJ}. (b) Lattice of cylindrical air holes with radius $R_c = 0.43a$ ($\varepsilon_a = 1, \varepsilon_b = 12$). The shaded bands show the TE PBGs, representing effective PBGs for G_{HM}.

with the EEM, it is found that the PAM is in excellent agreement with the EEM [27]. Moreover, with the PAM, G_{EJ} can be computed as efficiently as G_{HM}, while it is very delicate to process by the EEM [19] because of the non-Hermitian nature of the differential operator associated with the electric-field wave equation. Figs. 5(b)–10(b) show that, at excitation frequencies of the order of $\lambda/2$, convergence is reached with $N_G = 100$ for G_{EJ} and with $N_G = 300$ for G_{HM}, except at the position of the source where the Green's functions are singular. For G_{EJ}, N_G can be reduced to a very small value such as $N_G = 25$ without significant loss of accuracy, and $N_G = 10$ already provides a good idea of the shape of the Green's function for symmetry

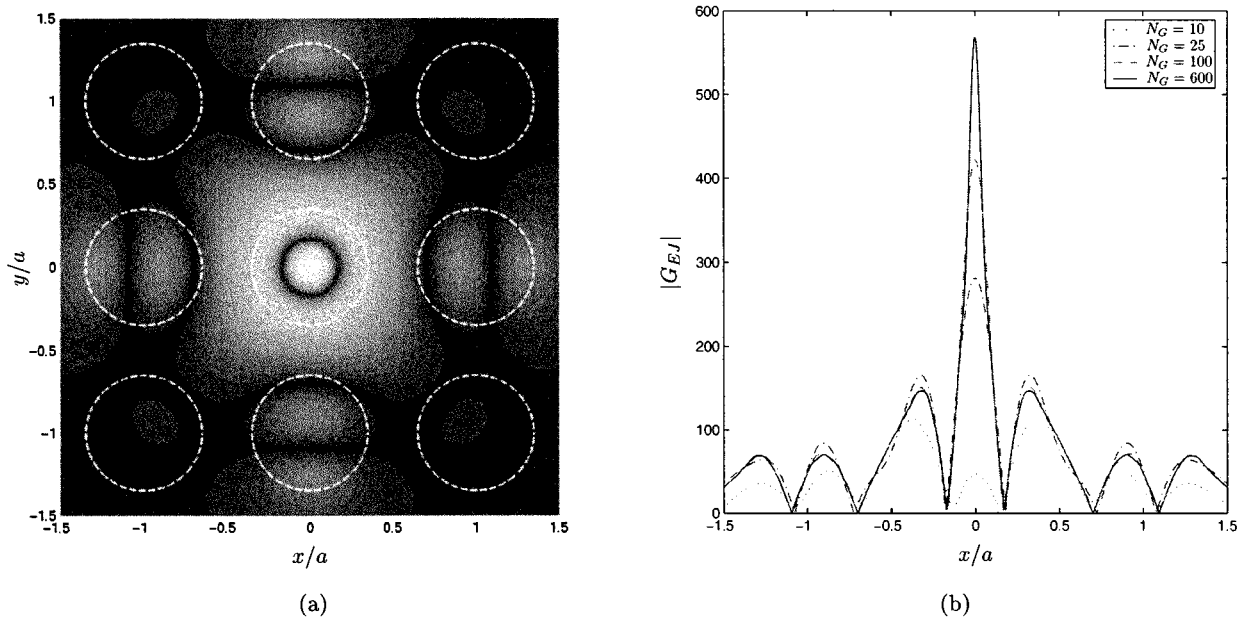

Fig. 5. Normalized Green's function $G_{EJ}(\boldsymbol{\rho}|\boldsymbol{\rho}')$ (modulus) for the source position $\boldsymbol{\rho}' = (0.0,\ 0.0)$ and excitation frequency $\omega_{\rm norm} = 0.42$ [$\in$ second TM PBG of Fig. 4(a)]. (a) 2-D view of $|G_{EJ}|$. (b) x cross section of (a) at $y = 0.0$.

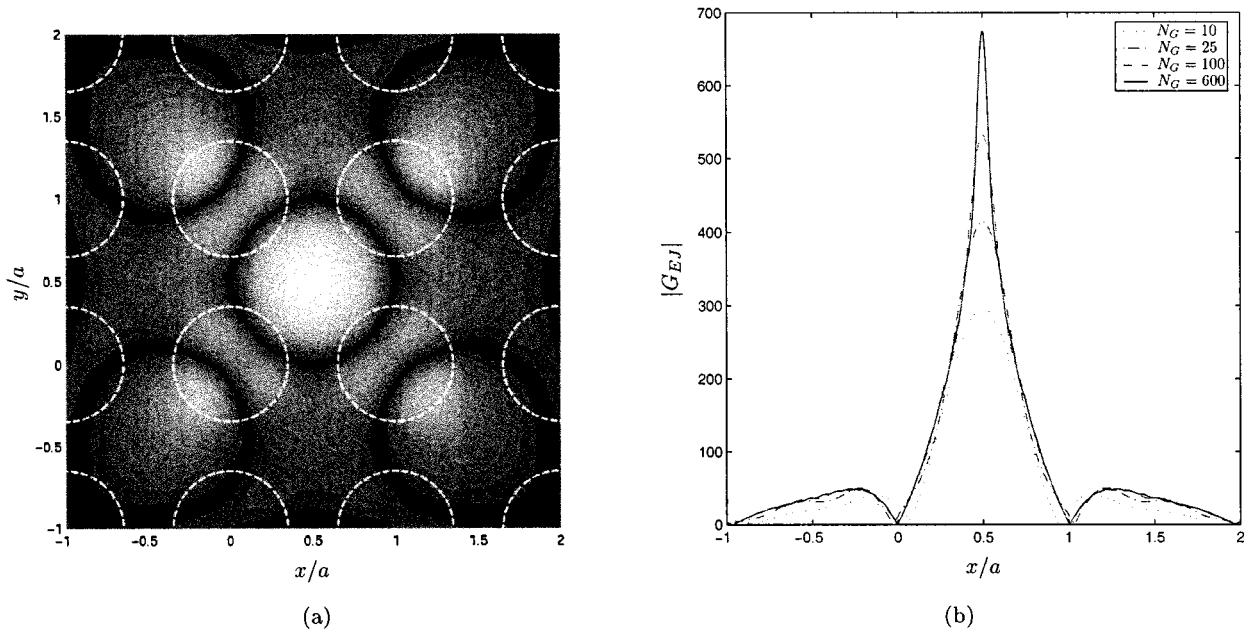

Fig. 6. Normalized Green's function $G_{EJ}(\boldsymbol{\rho}|\boldsymbol{\rho}')$ (modulus) for the source position $\boldsymbol{\rho}' = (0.5,\ 0.5)a$ and excitation frequency $\omega_{\rm norm} = 0.42$ [$\in$ second TM PBG of Fig. 4(a)]. (a) 2-D view of $|G_{EJ}|$. (b) x cross section of (a) at $y = 0.5$.

positions of the source. The fact that the convergence behaviors of G_{EJ} and G_{HM} are different can be explained by the dissymmetry of Maxwell equations in a PC, already mentioned in the previous section. It should be noted that N_G must be increased for frequencies lying in higher gaps, but in all the cases investigated, it has been found that $N_G = 300$ represents a sufficient number of plane waves.

The following physical characteristics of a PC excited by a localized source within a PBG can be inferred from the observation of the figures presented. Energy is highly confined in the vicinity of the source, which reveals the effect of the PBG. It is particularly concentrated in the dielectric areas of the PC where the permittivity is higher; this is explained by the trend of the fields to concentrate their energy in high-ε regions to lower their frequency [23]. The fields decay very rapidly as a function of the distance $|\boldsymbol{\rho} - \boldsymbol{\rho}'|$ from the source, which shows that electromagnetic waves are prevented from propagating and are totally reflected because of Bragg-like diffraction on the periodic structure. This feature is better emphasized in Figs. 11 and 12, which will be described in the following paragraph. As a consequence of Bragg-like diffraction, the fields take the form of standing waves, which are characterized by the presence of nodal points associated with phase inversion. In this regard, the PC acts in a manner that bears a strong resemblance with a classical cavity.

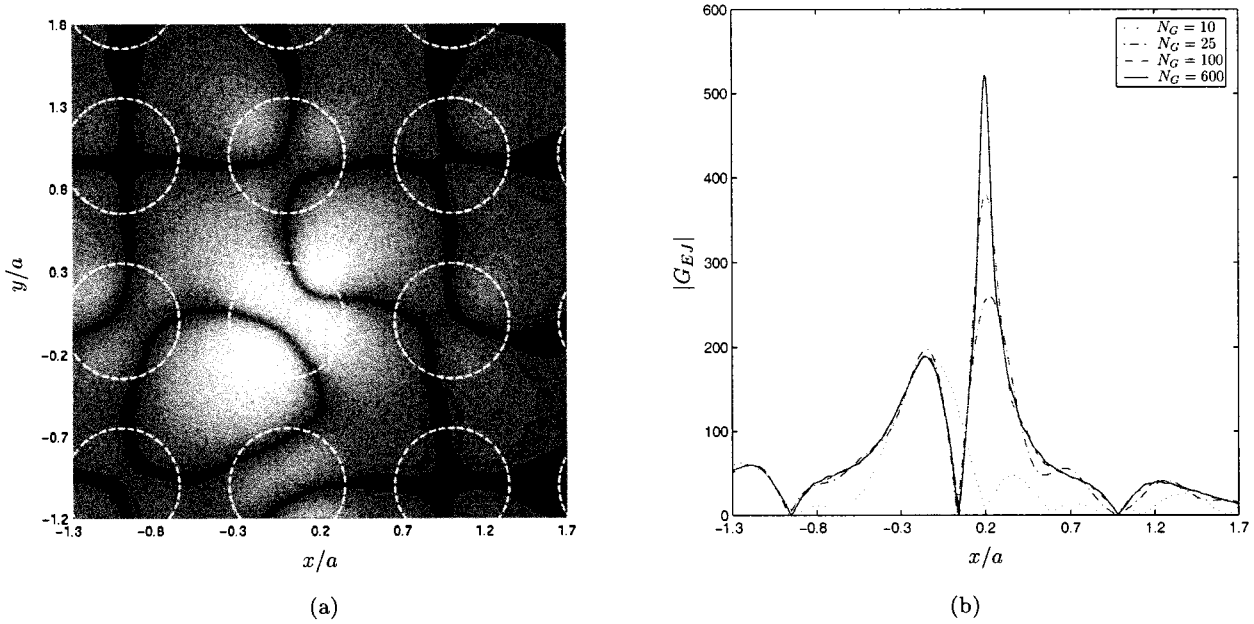

Fig. 7. Normalized Green's function $G_{EJ}(\boldsymbol{\rho}|\boldsymbol{\rho}')$ (modulus) for the source position $\boldsymbol{\rho}' = (0.2,\ 0.3)a$ and excitation frequency $\omega_{\rm norm} = 0.42$ [$\in$ second TM PBG of Fig. 4(a)]. (a) 2-D view of $|G_{EJ}|$. (b) x cross section of (a) at $y = 0.3$.

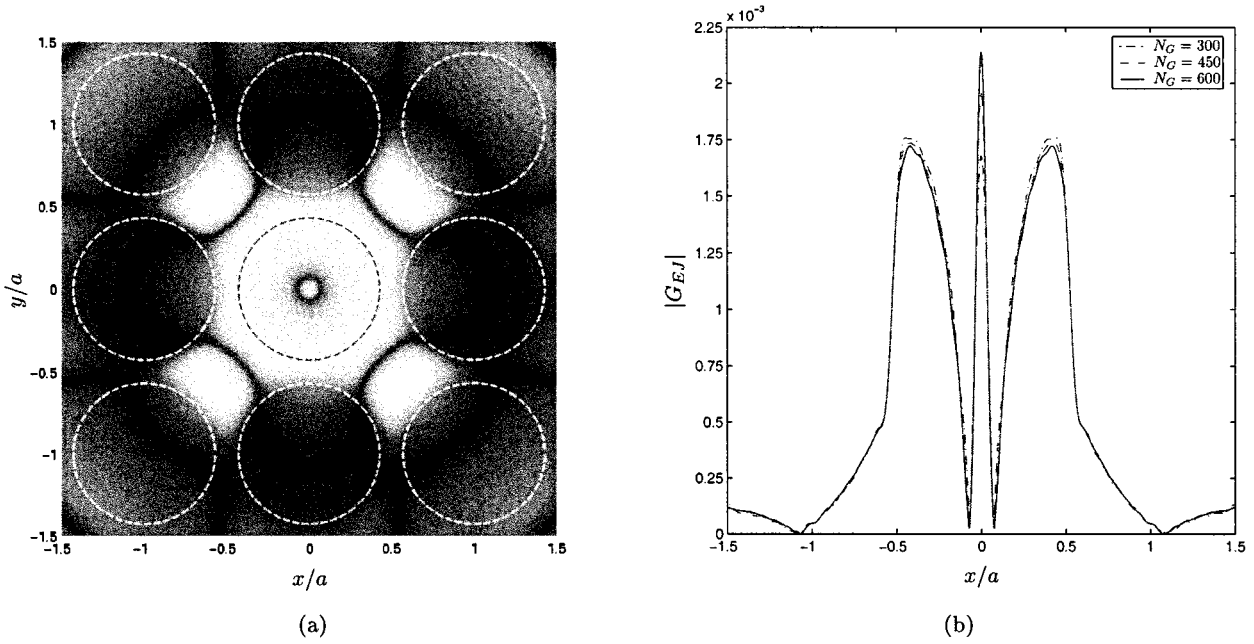

Fig. 8. Normalized Green's function $G_{HM}(\boldsymbol{\rho}|\boldsymbol{\rho}')$ (modulus) for the source position $\boldsymbol{\rho}' = (0.0,\ 0.0)$ and excitation frequency $\omega_{\rm norm} = 0.45$ [$\in$ second TE PBG of Fig. 4(b)]. (a) 2-D view of $|G_{HM}|$. (b) x cross section of (a) at $y = 0.0$.

Finally, as expected, the radiated fields reflect the symmetries of the crystal: whenever the source is located at a symmetry point, the Green's functions exhibit the same fourfold rotational symmetry as the crystal (Figs. 5, 6, 8, and 9), while they present dissymmetric patterns in the other cases (Figs. 7 and 10).

In all our computations, we have observed similar asymptotic behaviors for $|\boldsymbol{\rho} - \boldsymbol{\rho}'| \to \infty$ and $|\boldsymbol{\rho} - \boldsymbol{\rho}'| \to 0$. Figs. 11 and 12 show typical examples of the Green's functions away from the source ($|\boldsymbol{\rho} - \boldsymbol{\rho}'| \to \infty$), and also include for comparison the corresponding Green's functions in homogeneous media with the permittivity of the atoms (ε_a) of the background medium (ε_b) and of the volumetric average of the two ($\overline{\varepsilon}_r = \varepsilon_a f_r + \varepsilon_b(1 - f_r)$), respectively. It can be observed in these graphs that the Green's functions in the PC decrease much faster than in the homogeneous media, and fall to zero at a distance smaller than 2λ. This rapid vanishing of the fields, which is naturally attributed to the effect of the PBG, emphasizes the potential interest of PCs for filtering purposes in microstrip circuits and antennas. In the evaluation of the integral (2), attention must be paid to the fact that the Green's function, with (4), has a form reminiscent of an inverse Fourier transform (but is not exactly an inverse Fourier transform because the integrand also depends on

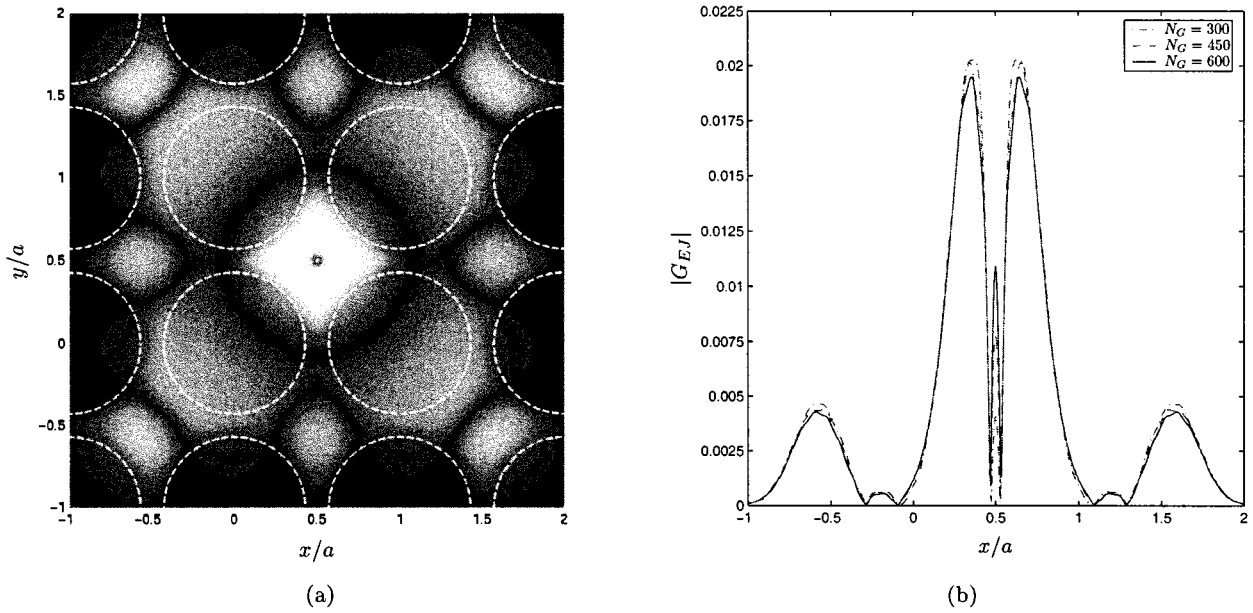

Fig. 9. Normalized Green's function $G_{HM}(\boldsymbol{\rho}|\boldsymbol{\rho}')$ (modulus) for the source position $\boldsymbol{\rho}' = (0.5,\ 0.5)a$ and excitation frequency $\omega_{\rm norm} = 0.45$ [$\in$ second TE PBG of Fig. 4(b)]. (a) 2-D view of $|G_{HM}|$. (b) x cross section of (a) at $y = 0.5$.

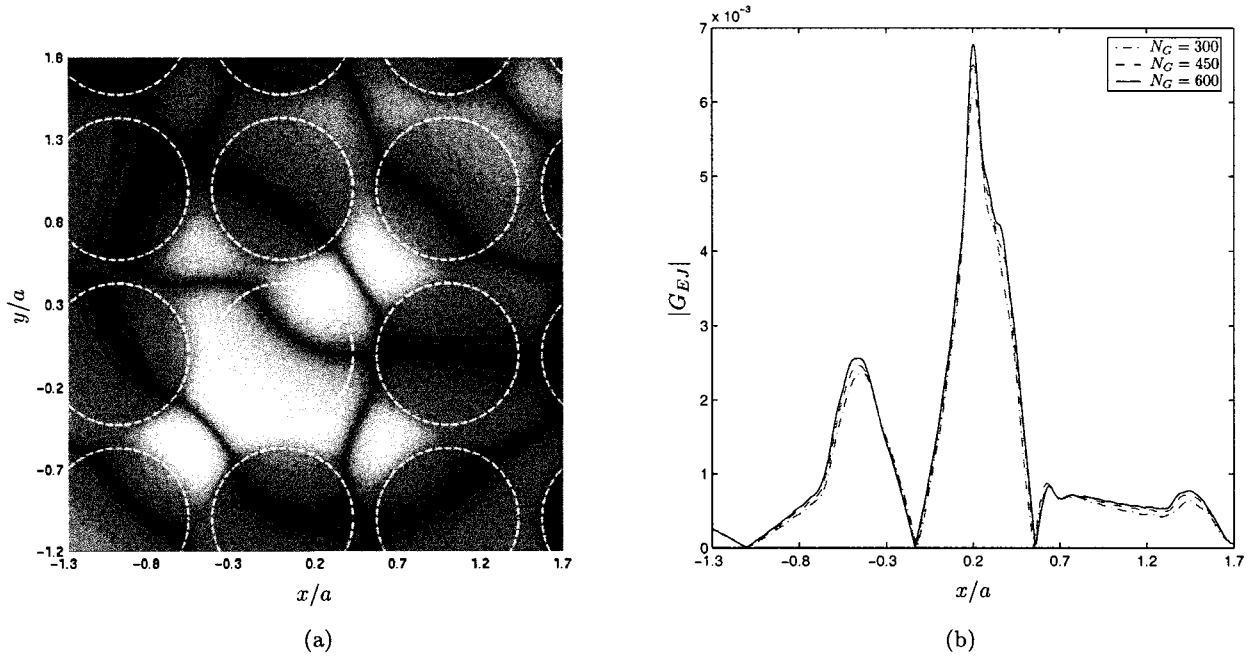

Fig. 10. Normalized Green's function $G_{HM}(\boldsymbol{\rho}|\boldsymbol{\rho}')$ (modulus) for the source position $\boldsymbol{\rho}' = (0.2,\ 0.3)a$ and excitation frequency $\omega_{\rm norm} = 0.45$ [$\in$ second TE PBG of Fig. 4(b)]. (a) 2-D view of $|G_{HM}|$. (b) x cross section of (a) at $y = 0.3$.

$\boldsymbol{\rho}$). As a consequence the Green's function, being the pseudoinverse Fourier transform of a sampled function, is a pseudoperiodic function, containing degenerated repetitions of the physical pattern localized near the source, and a sufficient number of integration points must be taken to avoid aliasing. In Figs. 11 and 12, with $N_k = 15$, the degenerated repetitions fall beyond the distance $\boldsymbol{\rho}/a = 5$ that is shown. Practically, the pseudoperiodic nature of the Green's function does not represent a problem for in-gap frequencies: As long as N_k is taken large enough to shift the repetitions of the physical pattern above the distance at which the field has vanished, the Green's function just has to be set to zero from that distance.

When the distance source observer tends to zero ($|\boldsymbol{\rho} - \boldsymbol{\rho}'| \rightarrow 0$), the Green's functions are singular, as in a homogeneous medium, for the 2-D problem considered [28]. Since the Bloch–Floquet expression of the periodic Green's functions (4) present no analytical poles at $\boldsymbol{\rho} = \boldsymbol{\rho}'$, the singularity of the Green's functions (12) at the position of the source follows only from the infinite ($N_G \rightarrow \infty$) Bloch–Floquet expansion. Numerically, we obtain finite values

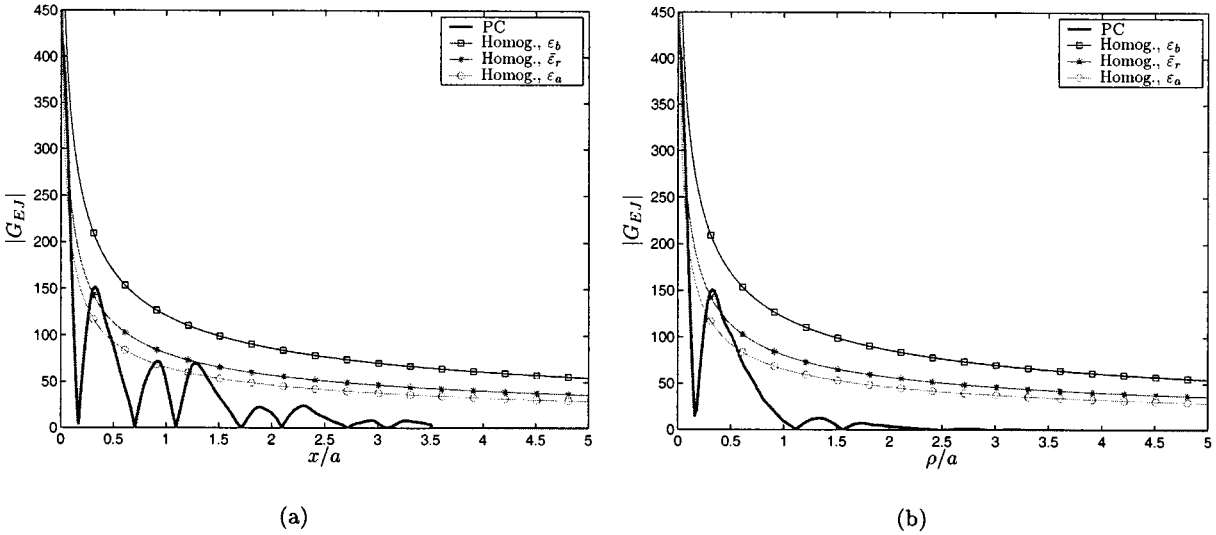

Fig. 11. Green's function $G_{EJ}(\boldsymbol{\rho}|\boldsymbol{\rho}')$ show in Fig. 5 ($\omega_{\rm norm} = 0.42 \in$ second TM PBG ($N = 100$, $N_k = 15$) farther from the source, compared with the corresponding Green's functions for homogeneous media of permittivites ε_a, ε_b, and $\bar{\varepsilon}_r$. (a) Cross section along the $\boldsymbol{e}_x$-direction, from $\boldsymbol{\rho}/a = (0.0,\ 0.0) = \boldsymbol{\rho}'/a$ to $\boldsymbol{\rho}/a = (5.0,\ 0.0)$. (b) Cross section along the $(\boldsymbol{e}_x + \boldsymbol{e}_y)$-direction from $\boldsymbol{\rho}/a = (0.0,\ 0.0) = \boldsymbol{\rho}'/a$ to $\boldsymbol{\rho}/a = (3.54,\ 3.54)$.

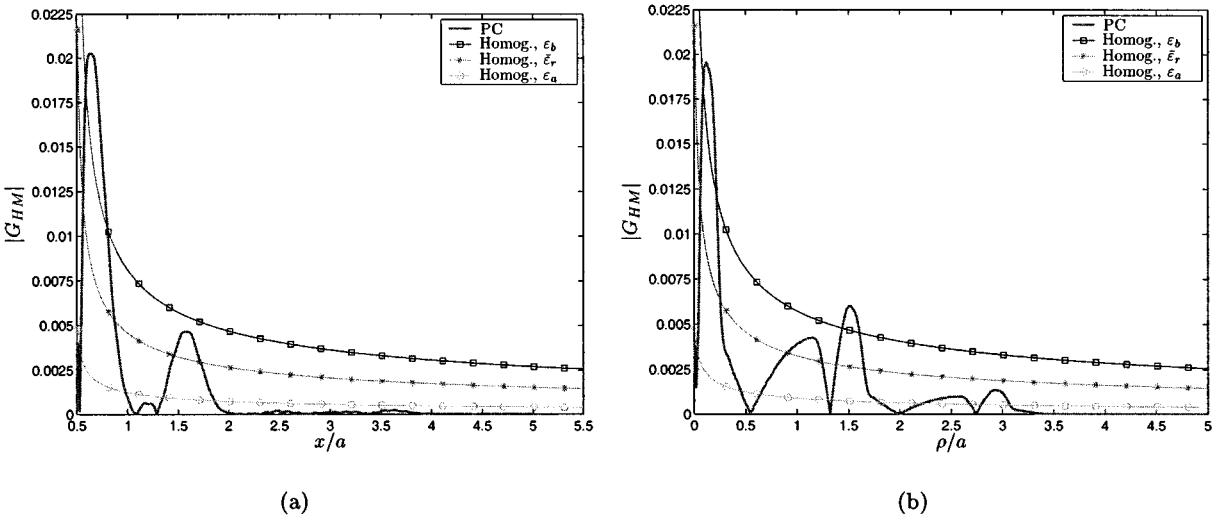

Fig. 12. Green's function $G_{HM}(\boldsymbol{\rho}|\boldsymbol{\rho}')$ show in Fig. 9 ($\omega_{\rm norm} = 0.45 \in$ second TM PBG) ($N = 300$, $N_k = 15$) farther from the source, compared with the corresponding Green's functions for homogeneous media of permittivites ε_a, ε_b and $\bar{\varepsilon}_r$. (a) Cross section along the $\boldsymbol{e}_x$-direction from $\boldsymbol{\rho}/a = (0.5,\ 0.5) = \boldsymbol{\rho}'/a$ to $\boldsymbol{\rho}/a = (5.5,\ 0.5)$. (b) Cross section along the $(\boldsymbol{e}_x + \boldsymbol{e}_y)$-direction from $\boldsymbol{\rho}/a = (0.5,\ 0.5) = \boldsymbol{\rho}'/a$ to $\boldsymbol{\rho}/a = (4.04,\ 4.04)$.

at $\boldsymbol{\rho} = \boldsymbol{\rho}'$ because the truncation of the expansion results in the suppression of high spatial frequency terms that are essential to represent the sharp diverging peak near the source. However, it can be seen in Figs. 5(b)–10(b) that the Green's functions exhibit a maximum (at least local) for any source position, and that this maximum increases monotonically with N_G, which reveals a singular behavior at the source position.

The Green's functions in the PAM formulation do not exhibit analytical poles, as in the EEM formulation. For this reason, the PAM might have been expected to be directly applicable for frequencies lying outside the PBGs. In fact, we have observed that the Green's functions become extremely unstable as soon as the excitation frequency penetrates into propagation regions of the photonic band structure. This nonconverging behavior for out-of-gaps frequencies shows that the PAM Green's functions contain numerical singularities, corresponding to the analytical poles of their EEM counterparts, and that the PAM is, therefore, not applicable without the addition of a procedure for the extraction of these singularities.

IV. Conclusions

A novel closed-form method to determine Green's functions in PCs, i.e., the PAM, has been proposed and developed in the case of a 2-D PC excited by an electric or magnetic current line. The PAM, which consists of a combination of the PWM and ASM, includes the information on periodicity in the Fourier coefficients of the permittivity as the EEM. However, it is a more efficient method than the EEM because it is stable for any field Green's function and because it is computationally much faster. Green's functions for different positions of the source inside the PC have been presented and several physical features of

radiation have been pointed out. In particular, the demonstration of the fast decrease to zero of the fields at in-gap frequencies has emphasized the filtering effect of the PBG. This paper represents a contribution to the study of Green's functions in PCs, and it is believed that the PAM, coupled with a standard method-of-moments procedure, will soon be applicable to the analysis of printed-circuit elements or antennas on PC materials.

Appendix I
Interpretation of the Wave Vector $\boldsymbol{k}_\rho$ in the PAM

In the context of the PC's theory, the wave vector $\boldsymbol{k}_\rho$ is essentially a *mathematical* wave vector that is adequate for the Bloch–Floquet expansion of the fields and can be restricted to the BZ by periodicity. It represents in no way a *physical* wave vector since such a vector can be defined only locally, either in the atoms or in the background medium. In the context of the phased-array theory, $\boldsymbol{k}_\rho$ enters in the phasing term $e^{j\boldsymbol{k}_\rho\cdot\boldsymbol{R}_\rho}$ of each source and, for finite sources dimensions, it is related to a scanning direction (θ, φ) given by the relation

$$\boldsymbol{k}_\rho = -k_0\left(T_x\mathbf{e}_x + T_y\mathbf{e}_y\right), \qquad \text{with } \begin{cases} T_x = \sin\theta\cos\varphi \\ T_y = \sin\theta\sin\varphi. \end{cases} \tag{13}$$

The PAM can be viewed as a combination of the two theories, in that $\boldsymbol{k}_\rho$ is present at the same time in the Bloch–Floquet expression of the fields [see (4)] and in the phasing factor of the sources [see (1) and (6)]. The wave vector $\boldsymbol{k}_\rho$ can thus be viewed as playing two distinct roles, which give rise to identical mathematical forms after application of the Poisson's sum formula to the array current.

Appendix II
Derivation of the Spectral Representation of the Phased-Array Current

The spatial expression of the phased-array current is given in (1) under the form

$$P_{\phi_\rho}(\boldsymbol{\rho}) = P_0\sum_{\boldsymbol{R}_\rho}\delta\left(\boldsymbol{\rho}-\boldsymbol{\rho}'-\boldsymbol{R}_\rho\right)e^{j\boldsymbol{k}_\rho\cdot\boldsymbol{R}_\rho} \tag{14}$$

where P_{ϕ_ρ} represents either J_{ϕ_ρ} or M_{ϕ_ρ}, and can be further written using the orthonormality property of the complex exponential as

$$P_{\phi_\rho}(\boldsymbol{\rho}) = P_0\sum_{\boldsymbol{R}_\rho} e^{j\boldsymbol{k}_\rho\cdot\boldsymbol{R}_\rho}\,\frac{1}{(2\pi)^2}\int_{-\infty}^{+\infty} e^{-j\boldsymbol{k}'_\rho\cdot\boldsymbol{\rho}'}e^{j\boldsymbol{k}'_\rho\cdot(\boldsymbol{\rho}-\boldsymbol{R}_\rho)}\,d\boldsymbol{k}'_\rho. \tag{15}$$

The Poisson's sum formula for a 2-D periodic function $f(\boldsymbol{\rho})$ [35] reads in the crystallographic formalism

$$S_{WSD}\sum_{\boldsymbol{R}_\rho} f\left(\boldsymbol{\rho}+\boldsymbol{R}_\rho\right) = \sum_{\boldsymbol{G}_\rho} e^{j\boldsymbol{G}_\rho\cdot\boldsymbol{\rho}}\tilde{f}\left(\boldsymbol{G}_\rho\right) \tag{16}$$

where S_{WSD} denotes the surface of the Wigner–Seitz cell of the direct lattice, and where the function $f(\boldsymbol{\rho})$ and its Fourier transform $\tilde{f}(\boldsymbol{k}_\rho)$ are related by the pair

$$f(\boldsymbol{\rho}) = \frac{1}{(2\pi)^2}\int_{-\infty}^{+\infty}\tilde{f}\left(\boldsymbol{k}_\rho\right)e^{j\boldsymbol{k}_\rho\cdot\boldsymbol{\rho}}\,d\boldsymbol{k}_\rho$$

and

$$\tilde{f}\left(\boldsymbol{k}_\rho\right) = \int_{-\infty}^{+\infty} f(\boldsymbol{\rho})e^{-j\boldsymbol{k}_\rho\cdot\boldsymbol{\rho}}\,d\boldsymbol{\rho}. \tag{17}$$

Now let $f(\boldsymbol{\rho}) = h(\boldsymbol{\rho})e^{j\boldsymbol{k}_{\rho_1}\cdot\boldsymbol{\rho}}$. Then $\tilde{f}(\boldsymbol{k}_\rho) = \tilde{h}(\boldsymbol{k}_\rho - \boldsymbol{k}_{\rho_1})$, and (16) becomes

$$S_{WSD}\sum_{\boldsymbol{R}_\rho} h\left(\boldsymbol{\rho}+\boldsymbol{R}_\rho\right)e^{j\boldsymbol{k}_{\rho_1}\cdot(\boldsymbol{\rho}+\boldsymbol{R}_\rho)} = \sum_{\boldsymbol{G}_\rho} e^{j\boldsymbol{G}_\rho\cdot\boldsymbol{\rho}}\tilde{h}\left(\boldsymbol{G}_\rho - \boldsymbol{k}_{\rho_1}\right) \tag{18}$$

or

$$S_{WSD}\sum_{\boldsymbol{R}_\rho} h\left(\boldsymbol{\rho}+\boldsymbol{R}_\rho\right)e^{j\boldsymbol{k}_{\rho_1}\cdot(\boldsymbol{\rho}+\boldsymbol{R}_\rho)} = \sum_{\boldsymbol{G}_\rho} e^{j\boldsymbol{G}_\rho\cdot\boldsymbol{\rho}}\int_{-\infty}^{+\infty} h\left(\boldsymbol{\rho}'\right)e^{-j(\boldsymbol{G}_\rho-\boldsymbol{k}_{\rho_1})\cdot\boldsymbol{\rho}'}\,d\boldsymbol{\rho}'. \tag{19}$$

At this stage, we notice that (15) and the right-hand side of (19) possess the same mathematical form, which suggests the dummy substitutions $\boldsymbol{G}_\rho \leftrightarrow \boldsymbol{R}_\rho$, $\boldsymbol{\rho} \rightarrow \boldsymbol{k}_\rho$ (and, therefore, $S_{WSD} \rightarrow S_{BZ}$), $\boldsymbol{\rho}' \rightarrow \boldsymbol{k}'_\rho$, and $\boldsymbol{k}_{\rho_1} \rightarrow \boldsymbol{\rho}$. Upon these substitutions, the relation (19) becomes

$$S_{BZ}\sum_{\boldsymbol{G}_\rho} h\left(\boldsymbol{k}_\rho+\boldsymbol{G}_\rho\right)e^{j(\boldsymbol{k}_\rho+\boldsymbol{G}_\rho)\cdot\boldsymbol{\rho}} = \sum_{\boldsymbol{R}_\rho} e^{j\boldsymbol{k}_\rho\cdot\boldsymbol{R}_\rho}\int_{-\infty}^{\infty} h\left(\boldsymbol{k}'_\rho\right)e^{j\boldsymbol{k}'_\rho\cdot(\boldsymbol{\rho}-\boldsymbol{R}_\rho)}\,d\boldsymbol{k}'_\rho. \tag{20}$$

The right-hand sides of (20) and (15) can be equaled, assuming that $h(\boldsymbol{k}'_\rho) = P_0e^{-j\boldsymbol{k}'_\rho\cdot\boldsymbol{\rho}'}/(2\pi)^2$. This finally yields the following spatial/spectral relation for the phased array current:

$$P_{\phi_\rho}(\boldsymbol{\rho}) = P_0\sum_{\boldsymbol{R}_\rho}\delta\left(\boldsymbol{\rho}-\boldsymbol{\rho}'-\boldsymbol{R}_\rho\right)e^{j\boldsymbol{k}_\rho\cdot\boldsymbol{R}_\rho} = P_0\,\frac{S_{BZ}}{(2\pi)^2}\sum_{\boldsymbol{G}_\rho} e^{j(\boldsymbol{k}_\rho+\boldsymbol{G}_\rho)\cdot(\boldsymbol{\rho}-\boldsymbol{\rho}')}. \tag{21}$$

Thus, this current possesses a Bloch–Floquet form, which can be written

$$P_{\phi_\rho}(\boldsymbol{\rho}) = P_0\,\frac{S_{BZ}}{(2\pi)^2}\sum_{\boldsymbol{G}_\rho}\tilde{P}\left(\boldsymbol{k}_\rho, \boldsymbol{G}_\rho\right)e^{j(\boldsymbol{k}_\rho+\boldsymbol{G}_\rho)\cdot\boldsymbol{\rho}} \tag{22}$$

where the $\boldsymbol{G}_\rho$–Bloch–Floquet coefficients $\tilde{P}(\boldsymbol{k}_\rho, \boldsymbol{G}_\rho)$ depend on the position $\boldsymbol{\rho}'$ of the zero-phased source and read $\tilde{P}(\boldsymbol{k}_\rho, \boldsymbol{G}_\rho) = \tilde{P}(\boldsymbol{k}_\rho + \boldsymbol{G}_\rho) = e^{-j(\boldsymbol{k}_\rho+\boldsymbol{G}_\rho)\cdot\boldsymbol{\rho}'}$.

REFERENCES

[1] E. Yablonovitch, "Inhibited spontaneous emission in solid-state physics and electronics," *Phys. Rev. Lett.*, vol. 10, no. 2, pp. 283–295, May 1987.

[2] *J. Mod. Opt. (Special Issue)*, vol. 41, no. 2, Feb. 1994.

[3] *Electromagnetics (Special Issue)*, vol. 19, no. 3, May/June 1999.

[4] *IEEE Trans. Microwave Theory Tech. (Special Issue)*, vol. 47, Nov. 1999.

[5] *J. Lightwave Technol. (Special Issue)*, vol. 17, Nov. 1999.

[6] T. F. Krauss, B. Vögele, C. R. Stanley, and R. M. D. K. Rue, "Waveguide microcavity based on photonic microstructures," *IEEE Photon. Technol. Lett.*, vol. 9, pp. 176–178, Feb. 1997.

[7] S.-Y. Lin, E. Chow, V. Hietala, P. R. Villeneuve, and J. D. Joannopoulos, "Experimental demonstration of guiding and bending of electromagnetic waves in a photonic crystal," *Science*, vol. 282, no. 5387, pp. 274–276, Oct. 1998.

[8] M. Boroditsky, R. Vrijen, T. F. Krauss, R. Coccioli, R. Bhat, and E. Yablonovitch, "Spontaneous emission extraction and Purcell enhancement from thin-film 2-D photonic crystals," *J. Lightwave Technol.*, vol. 17, pp. 2096–2112, Nov. 1999.

[9] O. Painter, A. Hussain, A. Scherer, J. D. O'Brien, I. Kim, and P. D. Dapkus, "Room-temperature photonic crystal defect lasers at near infrared wavelengths in InGaAsP," *J. Lightwave Technol.*, vol. 17, pp. 2082–2085, Nov. 1999.

[10] D. F. Sievenpiper and E. Yablonovitch, "Eliminating surface currents with metallodielectric photonic crystals," in *IEEE MTT-S Int. Microwave Symp. Dig.*, vol. 2, Baltimore, MD, June 1998, pp. 663–666.

[11] F.-R. Yang, Y. Qian, R. Coccioli, and T. Itoh, "A novel low-loss slow-wave microstrip structure," *IEEE Microwave Guided Wave Lett.*, vol. 8, pp. 372–374, Nov. 1998.

[12] I. Rumsey, M. Pilet-May, and P. K. Kelly, "Photonic bandgap structures used as filters in microstrip circuits," *IEEE Microwave Guided Wave Lett.*, vol. 8, pp. 336–338, Oct. 1998.

[13] R. Coccioli, F.-R. Yang, K.-P. Ma, and T. Itoh, "Aperture-coupled patch antenna on UC-PBG substrate," *IEEE Trans. Microwave Theory Tech.*, vol. 47, pp. 2123–2130, Nov. 1999.

[14] R. Coccioli and T. Itoh, "Design of photonic band-gap substrates for surface waves suppression," in *IEEE MTT-S Int. Microwave Symp. Dig.*, vol. 3, Baltimore, MD, June 1998, pp. 1259–1262.

[15] K. M. Ho, C. T. Chan, and C. M. Soukoulis, "Existence of a photonic band gap in periodic dielectric structures," *Phys. Rev. Lett.*, vol. 65, no. 25, pp. 3152–3155, Dec. 1990.

[16] M. Plihal, A. Shambrook, A. A. Maradudin, and P. Sheng, "Two-dimensional photonic band structures," *Opt. Commun.*, vol. 80, no. 3, 4, pp. 199–204, Jan. 1991.

[17] H.-Y. D. Yang, "Theory of antenna radiation from photonic band-gap materials," *Electromagnetics*, vol. 19, no. 3, pp. 255–276, May/June 1999.

[18] B. A. Munk and G. A. Burrell, "Plane-wave expansion for arrays of arbitrarily oriented piecewise linear elements and its application in determining the impedance of a single linear antenna in a lossy half-space," *IEEE Trans. Antennas Propagat.*, vol. AP-27, pp. 331–343, May 1979.

[19] T. Suzuki and P. K. Yu, "Emission power of an electric dipole in the photonic band structure of the FCC lattice," *J. Opt. Soc. Amer. B, Opt. Phys.*, vol. 12, no. 4, pp. 570–582, Apr. 1995.

[20] C. Caloz, D. Curcio, A. Alvarez-Melcon, A. K. Skrivervik, and F. E. Gardiol, "Slot antenna on a photonic substrate: Green's functions study," in *44th SPIE Annu.Terahertz Gigahertz Photon. Meeting Exhibition*, vol. 3795, Denver, July 1999, pp. 176–187.

[21] C. Kittel, *Introduction to Solid State Physics*, 7th ed. New York: Wiley, 1996.

[22] J. D. Joannopoulos, R. D. Meade, and J. N. Winn, *Photonic Crystals: Molding the Flow of Light*. Princeton, NJ: Princeton Univ. Press, 1995.

[23] R. D. Meade, A. M. Rappe, K. D. Brommer, and J. D. Joannopoulos, "Nature of the photonic band gap: Some insight from a field analysis," *J. Opt. Soc. Amer. B, Opt. Phys.*, vol. 10, no. 2, pp. 328–332, Feb. 1993.

[24] N. Amitay, V. Galindo, and C. P. Wu, *Theory and Analysis of Phased Array Antennas*. New York: Wiley, 1972.

[25] D. M. Pozar and D. H. Schaubert, "Scan blindness in infinite phased arrays of printed dipoles," *IEEE Trans. Antennas Propagat.*, vol. AP-32, pp. 602–610, June 1984.

[26] H. S. Sözüer and J. P. Dowling, "Photonic band calculations for woodpile structures," *J. Mod. Opt.*, vol. 41, no. 2, pp. 231–239, Feb. 1994.

[27] C. Caloz, A. K. Skrivervik, and F. E. Gardiol, "Green's functions in photonic crystals and their potential applications to microstrip antennas," in *Millenium Antennas Propagat. Conf.*, Davos, Switzerland, Apr. 2000, pp. 106–109.

[28] A. Q. Howard and D. B. Seidel, "Singularity extraction in kernel functions in closed region problems," *Radio Sci.*, vol. 13, no. 3, pp. 425–429, May/June 1978.

[29] E. R. Brown, C. D. Parker, and E. Yablonovitch, "Radiation properties of a planar antenna on a photonic crystal substrate," *Opt. Soc. Amer. B, Opt. Phys.*, vol. 10, no. 2, pp. 404–407, Feb. 1993.

[30] E. R. Brown and O. B. McMahon, "High zenital directivity from a dipole antenna on a photonic crystal," *Amer. Inst. Phys.*, vol. 68, no. 9, pp. 1300–1302, Feb. 1996.

[31] J. P. Dowling, M. Scalora, M. J. Bloemer, and C. M. Bowden, "The photonic band edge laser: A new approach to gain enhancement," *J. Appl. Phys.*, vol. 75, no. 4, pp. 1896–1899, Feb. 1994.

[32] C. M. Bowden, J. P. Dowling, and H. O. Everitt, "Development and applications of materials exhibiting photonic band gaps," *J. Opt. Soc. Amer. B, Opt. Phys.*, vol. 10, no. 2, Feb. 1993.

[33] R. K. Lee, O. J. Painter, B. Kitzke, A. Scherer, and A. Yariv, "Photonic bandgap disk laser," *Electron. Lett.*, vol. 35, no. 7, pp. 569–570, Apr. 1999.

[34] A. Mekis, J. C. Chen, I. Kurland, S. Fan, P. R. Villeneuve, and J. D. Joannopoulos, "High transmission through sharp bends in photonic crystal waveguides," *Phys. Rev. Lett.*, vol. 77, no. 18, pp. 3787–3790, Oct. 1996.

[35] A. Papoulis, *The Fourier Integral and its Applications*. New York: McGraw-Hill, 1962.

[36] V. Radisic, Y. Qian, R. Coccioli, and T. Itoh, "Novel 2-D photonic bandgap structures for microstrip lines," *IEEE Microwave Guided Wave Lett.*, vol. 8, pp. 69–71, Feb. 1998.

[37] M. M. Sigalas, R. Biswas, Q. Li, D. Crouch, W. Leung, R. Jacobs-Woodbury, B. Lough, S. Nielsen, S. McCalmont, G. Tuttle, and K. M. Ho, "Dipole antennas on photonic band-gap crystals—Experiment and simulation," *Microwave Opt. Technol. Lett.*, vol. 15, no. 3, pp. 153–158, June 1997.

[38] C. M. Soukoulis, Ed., *Photonic Band Gaps and Localization*. Norwell, MA: Kluwer, 1993.

[39] C. M. Soukoulis, Ed., *Photonic Band Gaps Materials*. ser. NATO ASI, E, App. Sci. Norwell, MA: Kluwer, 1996, vol. 308.

[40] P. R. Villeneuve, S. Fan, J. D. Joannopoulos, K.-Y. Lim, G. S. Petrich, L. A. Kolodziejski, and R. Reif, "Air-bridge microcavities," *Amer. Inst. Phys.*, vol. 67, no. 2, pp. 167–169, July 1995.

[41] P. R. Villeneuve, S. Fan, A. Mekis, and J. D. Joannopoulos, "Photonic crystals and their potential applications," in *IEE Semiconduct. Opt. Microcavity Devices Photonic Bandgaps Colloq.*, London, U.K., 1996, pp. 1–7.

[42] E. Yablonovitch, "Photonic band-gap structures," *J. Opt. Soc. Amer. B, Opt. Phys.*, vol. 10, no. 2, pp. 283–295, Feb. 1993.

[43] H.-Y. D. Yang, N. G. Alexopoulos, and E. Yablonovitch, "Photonic band-gap materials for high-gain printed circuit antennas," *IEEE Trans. Antennas Propagat.*, vol. 45, pp. 185–187, Jan. 1997.

[44] H.-Y. D. Yang, "Theory of microstrip lines on artificial periodic substrates," *IEEE Trans. Antennas Propagat.*, vol. 47, pp. 629–635, May 1999.

Christophe Caloz was born in Sierre, Switzerland, in 1969. He received the Diplôme d'Ingénieur en Électricité and the Ph.D. degree from the École Polytechnique Fédérale de Lausanne (EPFL), Lausanne, Switzerland, in 1995 and 2000, respectively.

In 2000, he joined the Microwave Electronics Laboratory, University of California at Los Angeles (UCLA), where he is currently an Assistant Research Engineer in the Electrical Engineering Department. His research interests include electromagnetic theory, numerical methods, planar circuits and antennas, PBG structures and left-handed (LH) materials.

Anja K. Skrivervik received the Electrical Engineering and Ph.D. degrees from the École Polytechnique Fédérale de Lausanne, Lausanne, Switzerland, in 1986 and 1992, respectively.

She was a Research Assistant at the Electromagnetics and Acoustics Laboratory, École Polytechnique Fédérale de Lausanne. In 1993, she spent six months as an Invited Scientist at the University of Rennes, where she began her activity on array analysis by supervising two Ph.D. students. From 1993 to 1995, she was involved with Swiss industry, where her research tasks were focused on antenna miniaturization and the development of electromagnetic field sensors. In 1995, she became an Assistant Professor for waves and radio communications at the École Polytechnique Fédérale de Lausanne. Her teaching activities include teaching microwaves and antennas. From 1996 to 2000, she was responsible for the electrical engineering undergraduate curriculum. Her research activities include the development of analysis for printed microwave structures, printed antenna array analysis, numerical techniques for electromagnetics, and the design and analysis of millimeter-wave antennas. She is active in European projects (Esprit, COST, ESA) and projects in collaboration with several companies.

Dr. Skrivervik was the recipient of a 1993 award of the Latsis Foundation for her doctoral thesis and research.

Fred E. Gardiol (S'68–M'69–SM'74–F'87–LF'01) was born in Switzerland, in 1935. He received the Physics Engineering degree from the École Polytechnique de l'Université de Lausanne, Lausanne, Switzerland, in 1960, the Masters degree in electrical engineering from the Massachusetts Institute of Technology, Cambridge, in 1965; and the Doctorate degree in applied science from the Catholic University of Louvain, Louvain, Belgium, in 1969.

From 1961 to 1966, he developed high-power microwave ferrite devices at the Special Microwave Devices Operation, Raytheon, Waltham, MA. He then joined Louvain University, Louvain, Belgium, where he became an Assistant Professor in 1969. From 1970 to 1999, he was a Professor and Director of the Laboratory of Electromagnetism and Acoustics (LEMA), École Polytechnique Fédérale de Lausanne, Lausanne, Switzerland. He has also been a Visiting Professor in Canada, Algeria, Brazil, India, Japan, France, and Italy. He authored (in French) *Électromagnétisme* (Laussanne, Switzerland: Presses Polytech. Univ. Romandes, 1996) (two versions) and *Hyperfréquences* (Laussanne, Switzerland: Presses Polytech. Univ. Romandes, 1981) and co-authored (in English) *Introduction to Microwaves* (Norwood, MA: Artech House, 1984), *Lossy Transmission Lines* (Norwood, MA: Artech House, 1987), *Microstrip Circuits* (New York, Wiley, 1994), *Broadband Patch Antennas* (Norwood, MA: Artech House, 1995), and *Engineering Applications of the Modulated Scatterer Technique* (Norwood, MA: Artech House, 2001). He has contributed over 300 technical publications on microwaves, loaded and open waveguides, microstrip circuits and antennas, and electromagnetic fields.

Dr. Gardiol is a member of the Swiss Electrotechnical Association, the Swiss Astronautics Association, the Massachusetts Institute of Technology (MIT) Club of Switzerland, and the Swiss Alpine Club. He was chairman of the IEEE Switzerland Section in 1975 and 1976. He founded the IEEE Swiss Joint Chapter of the IEEE Microwave Theory and Techniques Society (IEEE MTT-S) and the IEEE Antennas and Propagation Society (IEEE AP-S) in 1983. He was a member of the IEEE MTT-S Speakers Bureau from 1988 to 1989, and served on the Administrative Committee (AdCom) of the IEEE AP-S from 1988 to 1990. Since 1991, he has been an associate editor of the *IEEE Antennas and Propagation Magazine*. He chaired the Management Committee of the European Microwave Conference (EuMC) from 1973 to 1976, and organized the fourth EuMC in Montreux, Switzerland, in 1974. He chaired the Swiss National Committee of the International Radio Scientific Union (URSI) from 1980 to 1993, and Commission B of the International Scientific Radio Union (URSI) (Fields and Waves) from 1990 to 1993.